ISSN 0016-7029, Geochemistry International, 2007, Vol. 45, No. 10, pp. 957–970. © Pleiades Publishing, Ltd., 2007.
Original Russian Text © A.V. Ivanov, M.A. Ivanova, N.N. Kononkova, 2007, published in Geokhimiya, 2007, No. 10, pp. 1043–1056.

Concentrically Zonal Textures in a Sample of the Kaidun Meteorite

A. V. Ivanov, M. A. Ivanova, and N. N. Kononkova

Vernadsky Institute of Geochemistry and Analytical Chemistry, Russian Academy of Sciences, ul. Kosygina 19, Moscow, 119991 Russia

e-mail: andrei_ivanov@geokhi.ru

Received April 20, 2006

Abstract—The paper reports the results of the textural and mineralogical studying of clast Kaidun #d6A. The principal minerals of the clast are phyllosilicates, carbonates, and sulfides, but the clast contains no anhydrous silicates. The clast is characterized by extremely high concentration of inclusions, which broadly vary in size, composition, and texture, from completely remelted to practically unchanged when brought to the parent body. The latter group includes two inclusions having a concentrically zonal texture, which have never before been found in meteorites. One of the inclusions consists of serpentine replaced by talc in the margins. The inclusion was formed in relation to silification under the effect of silicon-bearing aqueous fluid at a temperature of more than 300°C. The other inclusion consists of alternating Ca carbonate and phyllosilicate zones. The texture and composition of the inclusion suggest that its genesis was related to the metasomatic alteration of carbonates under the effect of silicon- and alumina-bearing aqueous fluids at temperatures of about 400–500°C. These processes are typical of large differentiated planets, and there are no reasons to expect them in the parent bodies of carbonaceous chondrites, such as Kaidun. Our results obtained on clast #d6A are in good agreement with the hypothesis that the parent body of the Kaidun meteorite was Phobos [1]. Correspondingly, inclusions #d6Aa and #d6Ab likely originated from Mars, as previously examined alkali-rich clasts did. The clast described in this publication seems to originate from the surface regolith of Phobos, which was compacted in the process of the aqueous alteration of the material and subsequently buried at a greater depth.

DOI: 10.1134/S0016702907100011

INTRODUCTION

The Kaidun meteorite contains extremely diverse types of extraterrestrial material, including the products of processes that took place during the early preaccretionary evolution of the material (nebular condensation, gas metasomatism, agglomeration, and nebular melting), occurred in the parent body of the meteorite (impact melting, aqueous alterations, and material transfer), and were related to the magmatic differentiation of the material, as is typical of large enough planetary bodies [1–3].

This paper presents the results obtained by studying unusual clast #d6A, which was found in a polished thin section #d6 of a sample extremely rich in diverse inclusions.

METHODS

The material of the clast was examined by conventional techniques of optical microscopy and by scanning electron microscopy on CamScan. The composition of mineral phases was analyzed on a Camebax-microbeam microprobe. Most of the analyses were conducted at a current of 30 nA and an accelerating voltage of 15 kV. Mineral phases whose material evaporates when analyzed in standard mode were analyzed by rastering over areas 2×2 μm. The standards were natural minerals and synthetic compounds from the collection of standard housed at the Vernadsky Institute and borrowed from the Smithsonian Institution in Washington D.C., United States. ZAF corrections were applied to the results.

All phases present in the samples were identified based on their chemical analyses.

GENERAL CHARACTERIZATION OF CLAST #d6A

The morphology of clast #d6A (Fig. 1) can roughly be represented by a triangle with rounded corners and the largest dimension of 4 mm. A conspicuous feature of this clast is its extremely high content of foreign inclusions that are very diverse in composition and texture and range from 2 mm to a few dozen micrometers and less. In fact, it is quite difficult to find areas devoid of inclusions in this heterogeneous breccia.

The principal minerals of the clast are phyllosilicates, but it also contains widespread carbonates and sulfides and subordinate amounts of Fe oxides. No anhydrous silicates were detected in this clast.

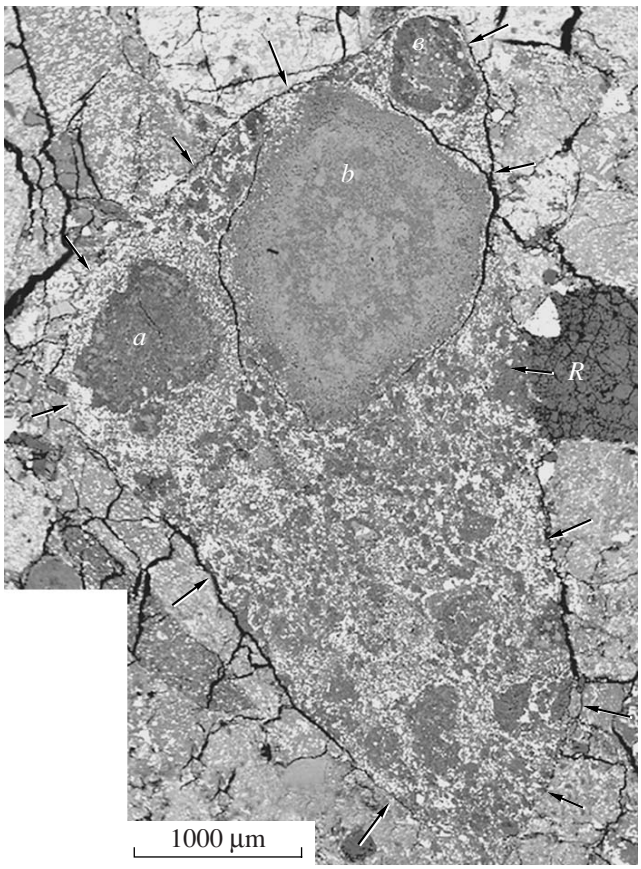

Fig. 1. BSE image of clast #d6A that is rich in inclusions. Letters *a*, *b*, and *c* mark the largest inclusions of the clast: #d6Aa, #d6Ab, and #d6Ac, respectively, *R* marks a sulfide–enstatite aggregate #d6R. Arrows point to the boundaries of clast #d6A.

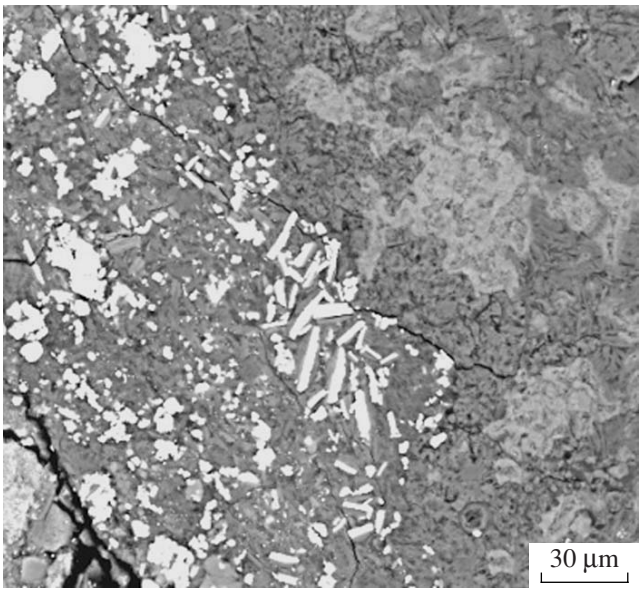

Fig. 2. BSE image of sulfide rim around inclusion #d6Aa. Elongated sulfide crystals are surrounded by thin phyllosilicate rims. Pale irregularly shaped blebs in the right-hand part of the image are ferrous serpentine in the talc zone of inclusion #d6Aa.

CLAST MATRIX

The major minerals of the matrix of the clast are phyllosilicates, sulfides are contained in lower concentrations, and Fe oxides are present in subordinate amounts.

The matrix phyllosilicates of the clast are, judging from the chemical composition (Table 1, analysis 1), dominated by magnesian serpentine. The high Al_2O_3 concentrations (~6 wt %) suggest that the serpentine is lizardite, which is characterized by the highest Al_2O_3 concentrations (up to 7 wt % and more) among the terrestrial polytypes of serpentine, whereas chrysotile and antigorite commonly contain no more than 1 wt % Al_2O_3 [4].

The matrix sulfides are presented mainly bound as abundant elongated crystals, up to 30 μm long and up to 8–10 μm thick. These crystals are ubiquitously present in the matrix and form rims around all inclusions contained in the clast (Fig. 2). The matrix also contains equant sulfide grains. Sulfides of both morphological types are usually strongly corroded and have uneven, strongly corroded surfaces. The Ni concentrations in the sulfides are 6–12 wt %, and their analytical totals are usually lower than 100%.

Elongate pyrrhotite crystals of morphology similar to that of sulfide crystals in our sample are quite typical of the Kaidun meteorite and were thoroughly examined in sample #01.3.18 [5]. The crystals in this sample are much larger than in sample #d6A but also compose rims around inclusions. It should be mentioned that pyrrhotite crystals of this habit in sample #01.3.18 are in fact polycrystalline aggregates with individuals <1 μm in size [5].

Many elongated sulfide crystals in our sample are covered, along their long axes, by phyllosilicate rims 3–5 μm thick (Fig. 2). The morphology of the rims is analogous to that of pyrrhotite in sample #01.3.18, although the rims in the latter are much thicker, up to 20 μm. The chemical composition of the rims is generally similar in both samples, but those in our sample contain less Fe and alkalis (table, analysis 2).

The similarities in the morphologies of sulfide crystals in sample #d6A and pyrrhotite crystals in sample #01.3.18, their similar concentrating around inclusions, and the occurrence of phyllosilicate rims in all of them suggest that they were produced by analogous (if not identical) processes. The high Ni concentrations in elongated sulfide crystals in sample #d6A can be accounted for by the oxidation of sulfides during aqueous alterations after their crystallization. Oxidation and passage into a dissolved state preferably affected Fe, whereas Ni, which is less prone to oxidation, should have enriched the remaining sulfide phase. The cor-

Chemical composition (averages and ranges, wt %) of the silicate components of fragment #d6A

Zone of inclusion	SiO_2	Al_2O_3	Cr_2O_3	FeO	MnO	MgO	CaO	Na_2O	K_2O	NiO	S	Total
Matrix of the fragment												
1. Matrix phyllosilicates (10)*	42.0 38.7–43.2	4.12 1.86–7.98	0.31 0.14–0.70	12.3 8.36–18.0	0.16 0.09–0.27	29.0 23.5–34.6	0.33 0.09–0.70	0.33 0.09–0.67	– <0.05–0.33	0.24 0.05–0.98	0.35 0.05–1.13	88.81
2. Rim of pyrrhotite lamellae (5)	38.0 37.1–39.5	5.95 5.59–6.29	0.90 0.72–1.11	12.7 11.8–14.0	0.11 0.06–0.15	28.2 27.2–29.1	0.10 0.09–0.14	0.22 0.20–0.26	0.09 0.06–0.12	0.41 0.26–0.61	0.92 0.57–1.56	87.60
Inclusion #d6Aa												
3. Core, serpentine (5)	42.1 40.6–43.7	2.05 1.65–2.58	– <0.05–0.07	9.00 7.96–9.78	0.19 0.12–0.37	34.0 32.2–37.2	– <0.05–0.06	– <0.05–0.10	– <0.05	– <0.05	– <0.05	87.34
4. Replacement front, serpentine (4)	41.0 40.2–42.5	2.20 1.18–3.22	– <0.05–0.11	12.4 11.6–12.9	0.42 0.37–0.51	31.9 29.0–33.0	0.05 0.05–0.06	– <0.05–0.09	– <0.05	– <0.05	– <0.05	87.97
5. Intermediate zone, talc (7)	60.4 59.3–61.3	0.53 0.45–0.63	– <0.05–0.11	4.74 4.05–5.39	– <0.05–0.11	27.3 25.6–28.8	0.11 0.05–0.30	0.15 0.12–0.20	– <0.05	– <0.05	– <0.05	93.23
6. Serpentine domains in talc (5)	37.9 36.2–38.7	4.19 3.93–4.58	0.12 0.05–0.25	22.9 22.1–24.3	0.17 0.11–0.23	22.8 21.8–23.8	0.14 0.09–0.20	0.21 0.16–0.28	– <0.05–0.06	– <0.05–0.07	– <0.05	88.43
7. Marginal zone, phyllosilicates (6)	42.3 40.3–45.7	2.76 1.95–4.05	0.17 0.05–0.48	11.3 9.43–13.9	0.24 0.17–0.46	30.6 26.0–34.6	0.10 0.05–0.15	0.20 0.11–0.45	0.06 0.05–0.16	0.06 0.05–0.07	– <0.05–0.11	87.79
Inclusion #d6Ab												
8. Serpentine (8)	39.0 36.7–40.4	4.17 2.69–5.35	– <0.05–0.29	12.1 10.4–13.7	0.25 0.17–0.40	32.1 28.4–34.1	0.16 0.08–0.22	– <0.05–0.16	– <0.05	– <0.05–0.16	– <0.05–0.06	87.78[2]*
9. Chlorite (9)	32.6 30.5–34.7	14.9 12.7–17.5	0.51 0.23–0.75	13.7 11.7–15.4	0.31 0.22–0.38	27.0 25.1–28.6	0.17 0.13–0.22	– <0.05–0.26	– <0.05	– <0.05–0.07	– <0.05–0.06	89.41[3]*
Inclusion #d6Ac												
10. Core, crystals (4)	42.3 41.8–42.8	2.15 2.12–2.20	0.53 0.50–0.58	10.6 10.4–10.9	0.32 0.27–0.34	31.7 31.0–32.3	– <0.05–0.07	0.17 0.13–0.20	– <0.05	– <0.05	– <0.05	87.77

Table. (Contd.)

Zone of inclusion	SiO_2	Al_2O_3	Cr_2O_3	FeO	MnO	MgO	CaO	Na_2O	K_2O	NiO	S	Total
11. Core, mesostasis (3)	34.5 34.1–34.7	10.5 10.0–10.8	0.21 0.17–0.28	14.2 13.2–15.0	0.21 0.15–0.26	25.3 24.8–26.4	0.21 0.12–0.39	0.30 0.29–0.32	– <0.05	0.10 0.05–0.14	0.08 0.07–.009	85.61
12. Rim, crystals (3)	39.1 38.6–40.3	2.26 1.98–2.50	0.66 0.52–0.75	9.63 7.89–10.9	0.24 0.21–0.27	29.1 28.1–29.7	0.08 0.07–0.10	0.15 0.11–0.18	– <0.05	0.08 0.06–0.10	0.06 0.06–0.07	81.36
13. Rim, mesostasis (3)	37.8 37.1–38.3	3.01 2.40–3.52	0.70 0.63–0.82	11.3 9.90–13.2	0.22 0.19–0.26	27.6 25.2–29.4	0.10 0.07–0.13	0.22 0.15–0.30	– <0.05	– <0.05–0.09	0.12 0.06–0.22	87.77
Inclusion #d6Ah												
14. Pseudocrystal (7)	40.9 38.8–42.9	2.65 1.65–3.71	0.39 0.14–0.66	10.8 8.29–12.4	0.24 0.17–0.36	31.5 28.9–35.0	0.13 0.08–0.19	0.12 0.08–0.14	– <0.05	– <0.05–0.12	– <0.05–0.10	86.73
15. Inclusion in crystal (6)	37.9 37.0–38.4	4.19 3.52–5.53	0.65 0.12–1.12	14.5 11.9–21.1	0.17 0.15–0.21	27.3 24.4–29.2	0.31 0.09–0.57	0.29 0.19–0.41	– <0.05–0.20	1.13 0.11–3.85	0.98 0.05–3.19	87.42
Inclusion #d6Ak												
16. Core (3)	39.4 38.1–40.6	4.65 4.38–4.79	0.56 0.37–0.75	17.5 16.9–18.2	0.19 0.17–0.21	29.1 28.2–29.6	0.81 0.46–0.99	0.27 0.26–0.28	0.08 0.07–0.09	1.19 1.11–1.31	1.17 1.01–1.26	94.92
17. Periphery (4)	44.1 43.1–44.9	1.98 1.80–2.20	0.12 0.05–0.25	10.0 7.77–11.8	0.15 0.11–0.18	36.0 34.6–37.4	0.10 0.05–0.17	0.09 0.08–0.10	– <0.05	0.41 0.07–1.32	 <0.05–0.08	92.95
Inclusion #d6Ad												
18. Serpentine (4)	42.1 40.1–43.4	1.95 1.71–2.18	0.12 0.08–0.17	9.44 8.46–10.3	0.18 0.14–0.23	34.3 32.1–35.8	0.11 0.05–0.22	0.05 0.04–0.06	– <0.05	– <0.05	– <0.05	94.92

Note: All Fe is recalculated to FeO;

* numerals in parentheses correspond to the number of analyses; the TiO_2 concentration is <0.05 wt % in all analyses except where indicated otherwise: [2]* including 0.05–0.10 wt % TiO_2; [3]* including 0.08–0.28 wt % TiO_2 (0.22 wt % on average).

roded surface of sulfide crystals in the sample is consistent with this explanation.

The practically ubiquitous presence of sulfide–phyllosilicate rims around foreign inclusions in the matrix definitely indicates that the matrix was the source of components for the rims and that the parameters of the aqueous fluid changed at the matrix–inclusion interface as a result of fluid interaction with the inclusions.

Iron oxides are presented by framboidal magnetite and irregularly shaped grains.

The matrix of clast #d6A shows similarities with the characteristics of carbonaceous chondrites of low petrological types.

Below we present characteristics of some inclusions in clast #d6A.

INCLUSION #D6Aa

Texture and Composition of the Inclusion

The inclusion has an irregular, almost equant shape (Fig. 3a) and sizes of 0.8×0.6 mm. The inclusion consists mostly of two phyllosilicates: serpentine and talc. The rare opaque minerals are sulfides. No carbonates were found in the inclusion.

Inclusion #d6Aa is zonal: its core is made up of serpentine with clearly pronounced crystal morphology (Fig. 3b). The next zone consists of talc. Near the boundary with serpentine, the material of this zone shows no features of crystallinity in SEM images. However, at some distance from this boundary, talc displays a typical felty morphology (Fig. 3c). The sharp sinuous boundary between the serpentine core and the talc zone is accentuated by a thin (3–6 μm) band of Fe-enriched serpentine, with the innermost part of this band being richer in Fe. Both of the zones are characterized by broadly varying apparent thicknesses. Both of them contain domains whose texture and composition corresponding to the other zone, which definitely reflects the complicated configuration of the boundary between the zones in the inclusion volume. The talc zone contains ferrous serpentine grains of irregular, amoeba-shaped morphology, which reach 80 μm (Fig. 2). In contrast to other mineral zones, the margin of the inclusion is characterized by a relatively constant thickness of 30–50 μm.

The inclusion is everywhere surrounded by a fine-grained sulfide–phyllosilicate rim 80–200 μm in apparent thickness (Fig. 2). The characteristics of the rim and its components were described above.

The compositions of phyllosilicates in inclusion #d6Aa are listed in the table (analyses 3–7). Note that the composition of the serpentine systematically varies from zone to zone of the inclusion: the FeO and Al_2O_3 concentrations increase and the MgO and SiO_2 concentrations decrease in the serpentine from the core (analysis 3) to the boundary between the core and interme-

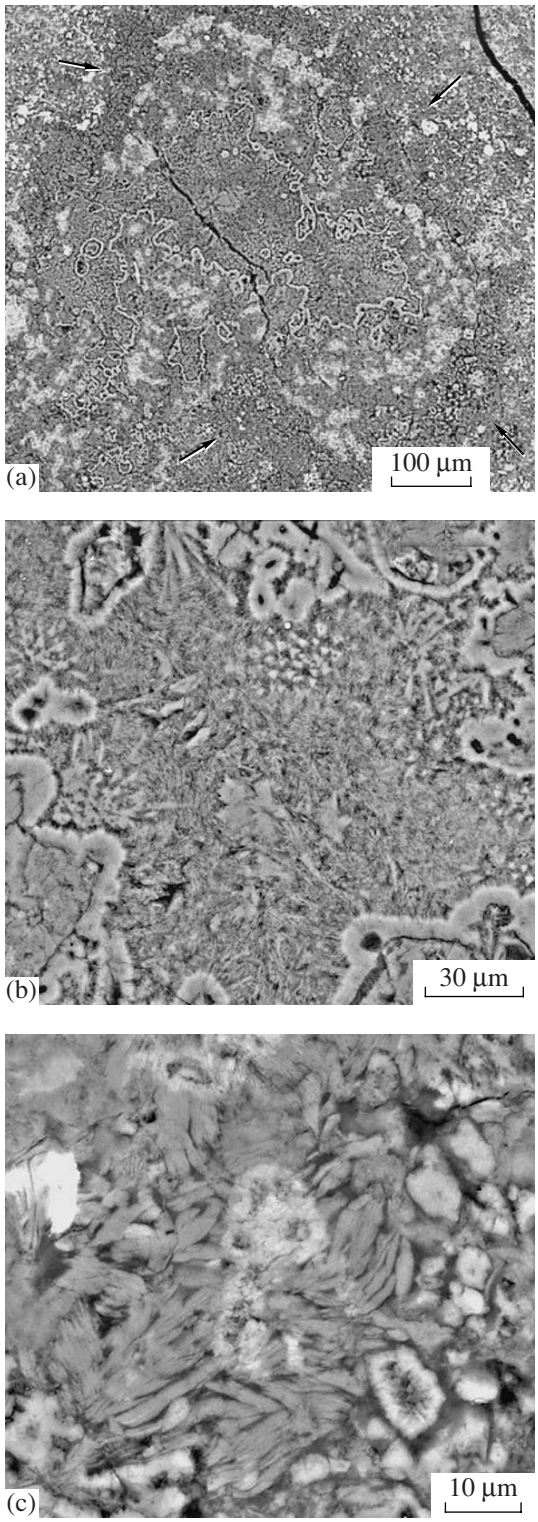

Fig. 3. BSE image of inclusion #d6Aa. (a) General view of the inclusion. The Mg-serpentine core is separated from the talc zone by a thin rim of Fe-enriched serpentine. (b) Morphology of serpentine in the core of the inclusion. (c) Morphology of talc in the inclusion. Pale patches are Fe-rich serpentine.

diate zone (analysis 4) and further to serpentine in the talc zone (analysis 6). The composition of talc in the inclusion (analysis 5) is analogous to that in terrestrial magnesian talc. The marginal zone of the inclusion consists of phyllosilicates of the serpentine series (analysis 7), whose composition differs from that of serpentine in other zones of the inclusion in having greater variations in the concentrations of most components.

Processes of the Inclusion Formation

Talc is a relatively rare mineral in meteorites. In some of them, its occurrence can be identified by TEM [5, 6]. The presence of sodic talc was documented in some metamorphosed carbonaceous chondrites, for example, Yamato-82162 [7] and Belgica-7904 [8]. However, the composition of sodic talc $NaMg_6(Si_7Al)O_{20}(OH)_4$ [7] is principally different from the composition of usual magnesian talc $Mg_3Si_4O_{10}(OH)_2$. We failed to find any published analyses of meteoritic talc of usual composition. The talc found in the sample is obviously the first talc of terrestrial type ever found in meteorites. The textures of serpentine replacement by talc analogous to those in our samples have never been documented before in meteorites.

Objects texturally close to inclusion #d6Aa were described in crystalline schists from California [9]. These are nodules ranging from 10 cm to >1 m in size that have spherical or ellipsoidal shapes. The cores of the nodules consist of serpentine and are surrounded by zonal rims, whose inner (closest to serpentine) zones are consists mainly of felty talc aggregates.

Talc can be formed in terrestrial rocks within broad temperature and pressure ranges: from conditions at the Earth's surface to 10 kbar and 900°C [4, 10]. Talc is often produced by contact metasomatism of ultrabasic rocks. In this processes, minerals are often replaced by talc after serpentinization, mostly under low metamorphic parameters (greenschist facies: 300–500°C, 3–8 kbar) [4, 11]. Talc can formed in insignificant amounts during the metamorphism of silicified dolomites. Talc was also found in hydrothermal veins with ore mineralization, in evaporites, and carbonate sediments.

The composition of talc produced under various conditions notably varies [11]. This mineral crystallizing in ultrabasic rocks contains FeO as the only admixture to the magnesian end member, normally in amounts of 1–4 mol % and never more than 13 mol %. The FeO concentration in talc formed in silicified dolomites does not exceed 5 mol %. Talc from hydrothermal and other low-temperature mineral assemblages is characterized by higher FeO concentrations.

The average FeO concentration in talc in inclusion #d6Aa is 5 mol % (table) and lies within the range of FeO concentrations typical of metamorphosed ultrabasic rocks.

Some textural features of the inclusion testify that its talc replaced serpentine. This follows from FeO and Al_2O_3 enrichment in the thin serpentine band at the boundary between the serpentine core and talc zone of the inclusion, particularly in the part of this zone closest to the serpentine core. The FeO and Al_2O_3 concentrations in the serpentine are notably higher than in usual magnesian talc. Serpentine replacement by talc results in the enrichment of the residual serpentine in these components at the boundary between the zones.

The replacement of serpentine by talc can proceed according to a number of schemes.

First, serpentine can be dehydrated and form forsterite [12, 13] by the scheme

$$5(Mg, Fe)_6[Si_4O_{10}](OH)_8 \longrightarrow 2(Mg, Fe)_3 \times [Si_4O_{10}](OH)_2 + 12Mg_2SiO_4 + 18H_2O. \quad (1)$$

However, the absence of any anhydrous silicates in the inclusion rules out this mechanism of talc formation.

Then talc can be formed by the carbonatization or silification according to one of the following principal schemes [14, 15]:

$$(Mg, Fe)_6[Si_4O_{10}](OH)_8 + 3CO_3 \longrightarrow (Mg, Fe)_3[Si_4O_{10}](OH)_2 + 3(Mg, Fe)CO_3 + 3H_2O, \quad (2)$$

$$(Mg, Fe)_6[Si_4O_{10}](OH)_8 + 4SiO_2 \longrightarrow 2(Mg, Fe)_3[Si_4O_{10}](OH)_2 + 2H_2O. \quad (3)$$

Neither breunnerite nor any other carbonates were detected in inclusion #d6Aa. Ca carbonates were found in some inclusions in clast #d6A, which are dominated by serpentine and contain no talc. These facts suggest that serpentine replacement by talc in inclusion #d6Aa is not related to in situ carbonatization according to reaction (2). However, this process cannot be ruled out for the previous parent body, before the inclusion occurred in its present setting.

Talc formation according to reaction (3) requires that silica was added to the system. We failed to identify any possible silica source either in inclusion #d6Aa itself or in the surrounding matrix. This means that the process of inclusion silification could not take place in situ (as also the carbonatization process could not). However, silification could occur in the previous parent body, before the inclusion was brought to its modern setting.

Hence, serpentine replacement by talc as a consequence of silification or carbonatization processes should have taken place in the previous parent body, before the inclusion appeared or was emplaced in its modern setting. The above comparison of the talc compositions in inclusion #d6Aa and in metamorphosed

terrestrial ultrabasic rocks (which were formed at silification) and silicified dolomites (produced by carbonatization) indicates that the silification process is more preferable.

The process of serpentine silification with the formation of talc is widespread in terrestrial rocks, when large masses of ultrabasic rocks are affected by contact metamorphism. Serpentine replacement by talc requires temperatures higher than 300°C [12], which is notably higher than the usual temperatures of aqueous alterations in CI (~85°C), CM (105–125°C), and CR (150°C) carbonaceous chondrites [16, 17].

The effect of high temperatures of about 500–700°C was identified in some thermally metamorphosed carbonaceous chondrites [18], including Yamato-82162 and Belgica-7904. At these high temperatures, serpentine is replaced by the association of talc + forsterite [19, 12]. Indeed, metamorphosed chondrites contain talc with forsterite. As was mentioned above, this talc is enriched in Na and Al and notably differs from magnesian talc widespread in terrestrial rocks and found in inclusion #d6Aa. Available data suggest that talc was formed in thermally metamorphosed carbonaceous chondrites according to scheme (1), i.e., via serpentine dehydration.

Serpentine replacement by talc in meteorites can also take place during the aqueous alterations of small volumes of ultrabasic material, for example, large olivine–pyroxene chondrules. Small talc amounts were found by TEM in chondrules of Allende [6]. However, the scale of this process should obviously have been very small, and the composition of the talc produced thereby was not reported.

Our data allowed us to propose a scenario for the genesis of inclusion #d6Aa. The alterations examined in this inclusion were related to the action of silica-bearing aqueous fluid. When talc replaced serpentine in the central zone, the excess FeO and Al_2O_3 enriched the serpentine at the alteration front of the boundary of the zones. The same process was likely responsible for the origin of ferrous serpentine in the talc zone, which can be regarded as a result of the final alteration stage of serpentine domains isolated in this zone during the alterations.

Serpentine silification is quite widespread in terrestrial rocks. At the same time, as was mentioned above, no traces of this process have ever been identified in meteorites. It is reasonable to believe that inclusion #d6Aa was formed at a fairly large planetary body that underwent deep differentiation of its material. This idea is in good agreement with the fact that the talc of the inclusion has a composition similar to that of terrestrial talc but notably different from the composition of talc in known meteorite samples.

The marginal zone of the inclusion notably differs from its inner zones, first of all, in having an unvarying thickness and inner texture and in showing no alterations typical of the inner parts of the inclusion. The serpentine composition in this zone differs from the composition of serpentine in both the core of the inclusion and the phyllosilicate matrix. Some characteristics of the marginal zone are similar to those of the so-called fine-grained rims or dust rims that surround many objects in carbonaceous chondrites. There are two groups of hypotheses proposed to explain the genesis of these rims. One of them explains the development of the rim in response to accretion processes prior to the emplacement of the object into chondrite [see, for example, 20]. According to the other group of hypotheses, the rim was produced by in situ aqueous alterations [see, for example, 21]. Available data did not allow us to choose between these hypotheses. However, in any event, the marginal zone of inclusion #d6Aa developed after the inner zones of the inclusion.

INCLUSION #D6Ab

Texture and Composition of the Inclusion

The inclusion has a roughly oval shape and sizes of 2.0 × 1.4 mm (Fig. 4a). The inclusion consists of Ca carbonate and phyllosilicates: serpentine and chlorite. The opaque minerals are rare magnetite grains. Anhydrous silicates are absent.

The texture of the inclusion is concentrically zonal, but its zones have no sharp boundaries and are distinguished by the predominance of certain minerals. The core of the inclusion is dominated by Ca carbonate. The following zone is made up of Ca carbonate and phyllosilicates, with the predominance of the latter. The third zone is dominated by Ca carbonate. The fourth, marginal zone is again dominated by phyllosilicates, and Ca carbonate is contained in subordinate amounts. The core of the inclusion contains serpentine and chlorite in commensurable amounts, whereas the fourth, marginal zone contains obviously more chlorite (Fig. 4b).

Inclusion #d6Ab, like that described above, is everywhere surrounded by a fine-grained sulfide–phyllosilicate rim, whose apparent thickness is approximately 60–80 μm.

The Ca carbonate grains vary in shape and size and are sometimes larger than 150 μm. Large grains display typical cleavage. Serpentine aggregates fill the interstitial space between Ca carbonate grains. The boundary between Ca carbonate and serpentine in the core of the inclusion often has a “crystallographic” configuration (Fig. 4c). Relatively small rounded grains of Ca carbonate in contact with serpentine are sometimes surrounded by thin (no thicker that 5 μm) serpentine rims, which is distinguishable by textural, but compositional, features. Chlorite is present only in serpentine aggregates, in which it forms relatively small (no more than 15 μm) grains of irregular, often amoeba-shaped, habit.

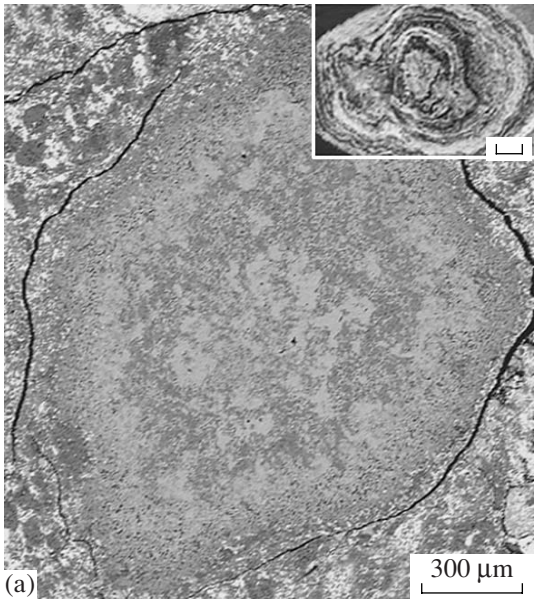

(a)

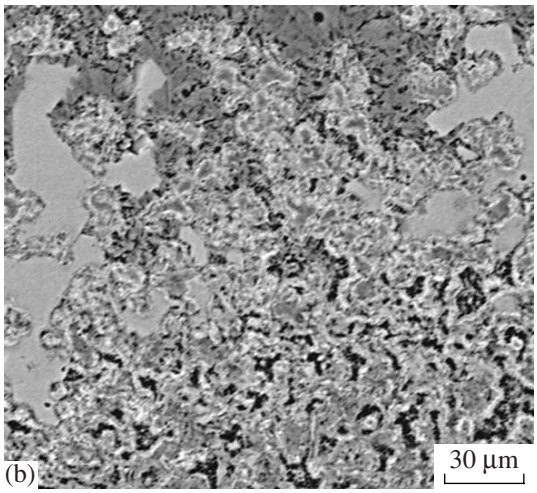

(b)

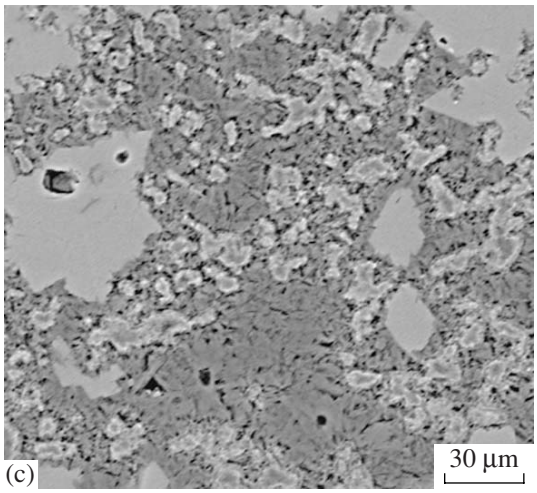

(c)

The compositions of serpentine and chlorite from inclusion #d6Ab are listed in the table (analyses 8 and 9). Various zones of the inclusion bear phyllosilicates of generally similar composition. Notable compositional variations of the phyllosilicates can be at least partly related to the mutual mixing of minerals in various proportions on a submicrometer scale. It is worth mentioning the systematic variations in the chemistry of the chlorite: chlorite in contact with serpentine is notably enriched in FeO compared to the central part, as is clearly pronounced in BSE images as pale rims in chlorite margins.

Ca carbonate in the inclusion contains very low Fe and Mg concentrations, which are pervasively accompanied by Si. The average concentrations (wt %) are 0.26 for Si, 0.44 for Fe, and 0.16 for Mg. There are good reasons to believe that the admixtures of these elements in the Ca carbonate are largely caused by the contamination with surrounding phyllosilicates.

Processes of the Inclusion Formation

Objects with textures and compositions analogous to those of inclusion #6dAb have never before been detected in meteorites. However, analogous rhythmically banded textures, including their concentrically zonal varieties, are quite usual in some terrestrial metasomatic rocks. They develop at contacts of carbonatite magmas with acid rocks [22] and are particularly characteristic of magnesian and calc skarns of the prograde stage of metamorphism (inset in Fig. 4) [23, 24].

The metasomatic alterations of carbonate rocks take place under the effect of magmatic fluids, which introduce Si, Al, and Fe. The mineralogy of the newly formed aggregates is controlled by several factors and largely depends on the temperature and pressure. According to the experimental data [25], obtained by modeling dolomite–granodiorite contact at a fluid pressure of 1 kbar and temperatures of 500–700°C, the inner-contact part includes the following zones: forsterite–forsterite + magnetite–forsterite + calcite. The

Fig. 4. BSE image of inclusion #d6Ab. (a) General view of the inclusion. Concentrically zonal texture of the inclusion is defined by the predominance of Ca carbonate (pale) and phyllosilicates (dark). The inset shows a concentrically zonal aggregate of alternating pyroxene and calcite bands. Specimen is from the collection of S.M. Aleksandrov, Tin Creek magnesian-skarn deposit, Lost River, Alaska. Scale bar is equal to 1 cm. (b) Marginal zone of the inclusion. Near the contact with the matrix (lower part of the image), the only phyllosilicate is chlorite, with serpentine appearing closer to the central part (dark patches in the upper part of the image). (c) Central zone of the inclusion. Some large Ca carbonate grains (pale) show rectilinear "crystallographic" boundaries with surrounding serpentine (dark gray). Smaller Ca carbonate grains have rounded morphologies and are surrounded by thin serpentine rims. Small amoeba-shaped grains are surrounded by pale rims of chlorite.

inner-contact part includes the following zones: clinopyroxene—clinopyroxene + plagioclase. As the temperature of the experiments was decreased to 550°C, the clinopyroxene concentration in the inner-contact zone decreased due to the development of amphibole, and the magnetite zone disappeared from the outer-contact part but an antigorite zone appeared in it. At a temperature of 400°C, the outer-contact part contains tremolite in association with antigorite in place of forsterite.

During the retrograde stage of metamorphism at the low-temperature alterations of skarns under the effect of aqueous solutions, the earlier silicates are replaced by serpentine and chlorite [24].

The development of mineral rhythms reflects an unequilibrated character of the process and occurs if the crystallization rates of the minerals are higher than the rate of solution supply. The minerals composing the rhythms show unchanging compositions. If thermodynamic equilibrium is reached, the rhythms are disordered up to complete disappearance [24].

The characteristics of rhythmically banded terrestrial metasomatic rocks and inclusion #d6Ab in the Kaidun meteorite led us to hypothesize that the genesis of the latter was related to the metasomatic alterations of carbonates. This follows, first of all, from the obvious textural similarities between inclusion #d6Ab and analogous aggregates in terrestrial metasomatic rocks, as well as the mineralogy of the rhythms, and the constancy of mineral compositions in them. The "diffuse" character of the rhythms likely suggests that the mineral system of the inclusion approached thermodynamic equilibrium.

The data presented above on the inner structure and composition of inclusion #d6Ab in comparison with experimental data [25] and the results of petrological studies [23] allowed us to draw some provisional conclusions concerning the genesis of the inclusion. The absence of the magnetite zone from the inclusion likely suggests that the temperature of the metasomatic alteration was no higher than 550°C. At this temperature, both pyroxene (diopside) and amphibole can crystallize. The further low-temperature aqueous alterations resulted in the replacement of the newly formed silicates by serpentine and chlorite.

The predominant restriction of chlorite to the marginal zone of inclusion #d6Ab and the morphology of the chlorite aggregates replacing serpentine quite definitely indicate that chlorite, or its precursor, was formed during the final evolutionary stage of the inclusion in the presence of water. The comparison of the compositions of the serpentine and chlorite (table, analyses 8, 9) indicates that a noteworthy characteristic of the fluid was its elevated concentrations of Al_2O_3, Cr_2O_3, and TiO_2. This association is mobile in acidic aqueous fluid at pH < 5 (under standard conditions) [26], i.e., occurred during the acidic stage of the aqueous phase of alterations at temperatures of 200–400°C [22].

The character of the matrix of clast #d6A and its mineralogical and chemical composition rule out the possibility of in situ formation of inclusion #d6Ab. This inclusion, like inclusion #6dAa described above, was produced outside clast #d6A and was emplaced into it during its later evolutionary history.

INCLUSION #D6Ac

Texture and Composition of the Inclusion

The inclusion (Fig. 5) has a round morphology and is approximately 0.5 mm across. It is dominated by hydrated silicates of various composition. The opaque minerals are Fe sulfides. Similarly to all other inclusions in this clast, this inclusion is surrounded by a fine-grained sulfide–phyllosilicate rim.

The inclusion is zonal, as can be clearly seen in the BSE image (Fig. 5). Its core approximately 0.3 mm across has a porphyritic texture and consists of equant crystals up to 50 μm across submerged in a massive vitreous mesostasis. The rim is made up of elongated skeletal crystals up to 120 μm in a porous mesostasis.

The compositions of the components of inclusion #6dAc are listed in the table (analyses 10–13). The lower analytical totals of the rim of the inclusion compared with the totals for the core can likely be explained by the porous texture of the rim.

The composition of crystals in the core is practically unvarying, and skeletal crystals in the rims show notable compositional variations, perhaps, mostly because of their morphology. At the same time, the average compositions of crystals in both structural settings are closely similar, and their concentrations of major elements are identical, which follows from the constancy of their ratios: the SiO_2/FeO ratio in crystals from the core and rims is equal to 4.0 and 4.1, respectively, and the SiO_2/MgO ratio is equal to 1.3 for both of them. The composition of crystals in both zones corresponds to serpentine, but their morphologies are atypical of this mineral. These crystals obviously resulted from the aqueous alteration of earlier silicates. Skeletal olivine crystals are very typical of rapidly cooling meteorite chondrules. Conceivably, olivine was a primary mineral in the inclusion.

Compared with the corresponding mesostasis, the crystals of the inclusion in various settings are enriched in SiO_2, MnO, and MgO but depleted in Al_2O_3, FeO, CaO, and Na_2O, and the differences between the compositions of the components of the core are more significant that those of the components of the rim.

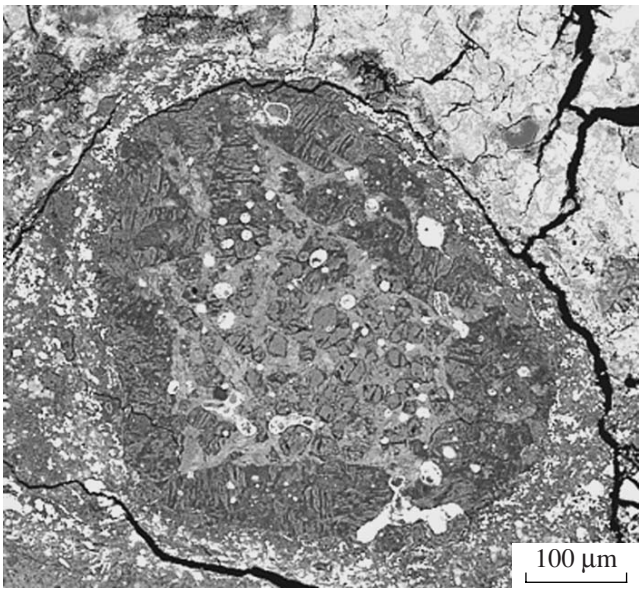

Fig. 5. BSE image of inclusion #d6Ac with a zonal texture.

Processes of the Inclusion Formation

The porphyritic texture of inclusion #d6Ac, which is defined by crystals in a vitreous mesostasis, obviously indicates that the inclusion was produced by the crystallization of melt, and the rounded morphology of the inclusion indicates that the melt solidified in free space. The zonal texture of the inclusion suggests that its core and rim crystallized with notably different rates: the rim with skeletal crystals crystallized when the melt rapidly cooled, whereas the core of the inclusion crystallized at slower cooling.

Available data led us to propose the following scenario for the genesis of inclusion #d6Ac. The melt produced by a high-velocity impact was ejected in the form of a droplet. The in-flight cooling of the melt via irradiation resulted in the cooling of the droplet at the surface, its further crystallization in the form of a rim with skeletal crystals. Upon the fall of the partly solid particle onto the surface of the parent body of the meteorite, the particle was overlain by crater ejecta, which were most probably produced by the same impact event that formed the melt particle itself. Its further crystallization proceeded in the regolith, when the droplet cooled more slowly. The material was then affected by aqueous alterations in the parent body of the meteorite.

SMALL INCLUSIONS

As was mentioned above, clast #d6A is extremely rich in inclusions of broadly variable size. This section presents a brief characterization of some small inclusions in this clast that differ in composition and texture.

Inclusion #d6Ah (Fig. 6a) shows a clearly pronounced crystalline habit and has sizes of 140×60 μm. The "crystal" contains an oval inclusion 30×25 μm. Both components consist of phyllosilicates. The "crystal" itself can evidently be regarded as a pseudomorph of phyllosilicates after a crystal of some Fe–Mg silicate.

Judging from the morphology of the pseudomorph, the precursor crystal could be either olivine or pyroxene. The pseudomorph is relatively rich in Cr_2O_3 (up to 0.66 wt %) which is atypical of terrestrial olivine. However, these concentrations are quite common in meteoritic olivine, including this mineral in the Kaidun meteorite [27]. Other chemical elements of the pseudomorph were relatively mobile during the aqueous alterations of the silicates. Hence, available data are insufficient for determining the mineral type of the original crystal.

As can be seen in the BSE images and follows from chemical analyses, the oval inclusion in the crystal (Fig. 6a) was polymineralic and contained, along with a silicate phase (or phases), also Fe, Ni-sulfide. The silicate component of the oval inclusion is enriched in some minor elements (Al_2O_3, CaO, Na_2O, and K_2O) compared to the material of the crystal.

Inclusion #d6Ak (Fig. 6b) 100 μm across has a roughly equant shape and a zonal inner texture. Both of its zones are composed of hydrated silicates and contain grains of Fe hydroxides and Fe, Ni-sulfides. The rim of the inclusion contains relatively rare and large (usually >2 μm) grains of opaque minerals, while the core contains two groups of grains: along with relatively large rare grains similar to those in the rim, it contains abundant submicrometer-sized grains of Fe oxides.

Olivine and pyroxene containing submicrometer-sized grains of metallic Fe (so-called "dusty grains") are quite common in the chondrules of ordinary chondrites and were also detected in carbonaceous CM and CV chondrites [28, 29]. Their genesis is thought to have been related to the reduction of Fe-rich silicate grains at changes in the redox conditions. The situation in the inclusion is similar to that in "dusty grains", although the opaque phase in it is Fe oxides. It is reasonable to think that the mechanism that produced the submicrometer-sized opaque phase in the inclusion was analogous to the mechanism responsible for the origin of "dusty grains", but the metal of the submicrometer-sized phase was then oxidized during the aqueous alteration of the material.

The compositions of the silicate component in the core and rim of the inclusion are notably different. The core is rich in FeO (18 wt %), NiO (2.5 wt %), and S (1.8 wt %). For at least the latter two components, this can be caused by the incorporation of tiny sulfide grains. Moreover, the core of the inclusion is notably

enriched in minor elements (up to 5 wt % Al_2O_3, up to 2.5 wt % CaO, and up to 0.4 wt % Na_2O) compared to the rim (no more than 2.5 wt % Al_2O_3, no more than 0.2 wt % CaO, and no more than 0.15 wt % Na_2O).

The genesis of inclusion #d6Ak was likely related to the melting of multiphase material without homogenization of the resultant melt and with the subsequent aqueous alteration of the material.

Inclusion #d6Ad (Fig. 6c) has a maximum size of 260 μm and is characterized by an irregular shape. It consists of magnesian serpentine and Ca carbonate and contains subordinate amounts of pyrrhotite, which can be hosted in both serpentine and Ca carbonate. The serpentine is loose in the core of the inclusion and massive in its margins. The Ca carbonate of this inclusion is characterized, like this mineral in inclusion #d6Ab, by low concentrations of minor elements. It is worth mentioning that clast #d6A contains a few inclusions of this type.

The texture of the inclusion indicates that it was not melted when brought to the parent body but underwent aqueous alterations, which resulted in the compaction of the serpentine texture in the marginal zone of this inclusion.

GENESIS OF CLAST #D6A AND ITS INCLUSIONS

The absence of anhydrous silicates from all components of clast #d6A testifies that the material of this clast underwent quite extensive aqueous alterations. The texture of the clast, for example, the occurrence of sulfide rims around practically all inclusions in this clast and the development of outer rims around some of the inclusions (#d6Aa and #d6Ad), suggests that the inclusions were affected by aqueous alterations already in the clast. This does not mean that these alterations were the only ones in the evolutionary history of the clast. Moreover, it shows undeniable evidence of the earlier aqueous alterations of at least some of its components. This is, for example, inclusion #d6Aa, which was produced under the effect of silica-rich aqueous fluid, a process that could not take place in the carbonaceous chondritic parent body of the meteorite.

It is important to note that the aqueous alteration of clast #d6A and its components took place before the clast was emplaced in its modern setting. This definitely follows from the occurrence of sulfide–enstatite aggregate #d6R at immediate contact with clast #d6A (Fig. 1). Aggregates of this type were also found in other thin sections of the Kaidun meteorite [30]. They consist of pure enstatite with inclusions of rare sulfides: niningerite and heideite. These minerals, first of all, sulfide, should have been inevitably affected by significant alterations if the extensive aqueous transformations of clast #d6A occurred in situ.

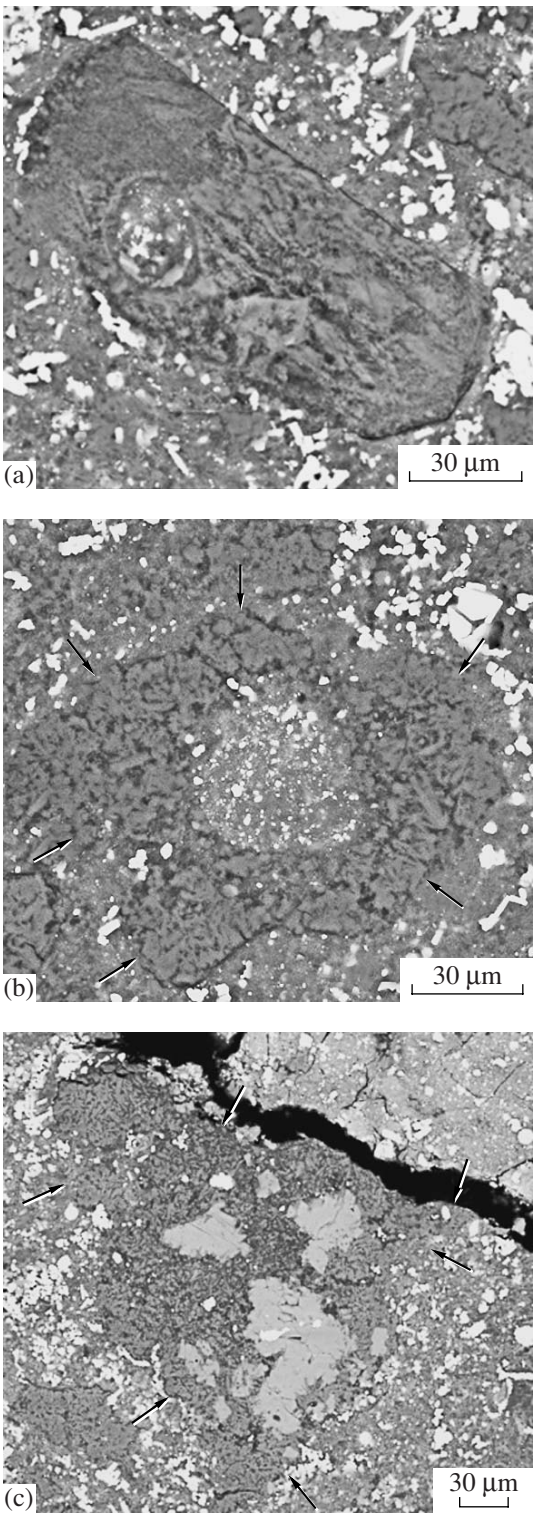

Fig. 6. BSE image of small inclusions in clast #d6A. (a) Inclusion #d6Ah. Pseudomorph of phyllosilicates after a crystal of a Fe–Mg silicate. (b) Phyllosilicate inclusion with core #d6Ak enriched in opaque minerals. (c) Phyllosilicate inclusion with calcite and sulfide #d6Ad. Arrows point to the boundaries of the inclusion.

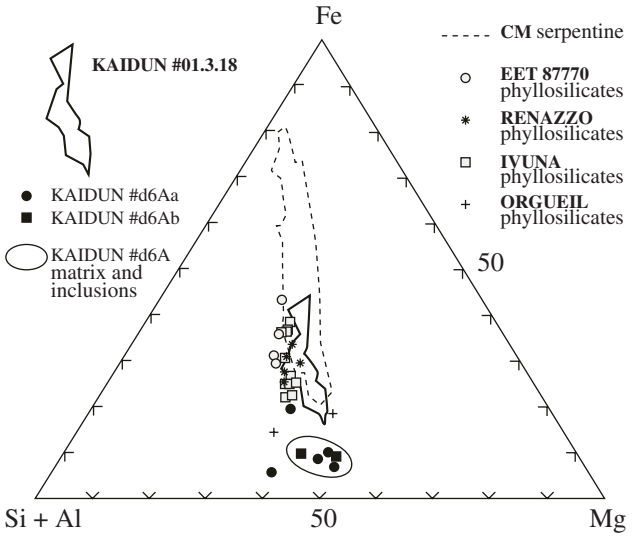

Fig. 7. Average composition of phyllosilicates in inclusions #d6Aa and #d6Ab and the compositional field of the matrix and small inclusions of clast #d6A plotted in a Fe–Mg–(Si + Al), at %, diagram. The diagram also shows the field of serpentine in CM chondrites and the compositions of phyllosilicates in CI1 (Ivina and Orgueil) and CR2 (EET 87770 and Renazzo) chondrites and the compositional field of phyllosilicates in sample Kaidun #01.3.18. The diagram is modified after [5].

Similarly to the Kaidun meteorite as a whole, the clast contains inclusions that arrived at the parent body with significantly different velocities. For example, along with inclusions showing traces of melting (for example, #d6Ac and #d6Ak), which collided with the parent body having velocities of a few kilometers per second [31], the clast also contains inclusions that display practically no traces of impact metamorphism (for example, #d6Aa and #d6Ab), which arrived at the parent body having practically zero velocities.

A noteworthy feature is the much more magnesian composition of phyllosilicates in clast #d6A compared to phyllosilicates in CI, CM, and CR chondrites and the matrix of clast Kaidun #01.3.18 [5] (Fig. 7). The unusually high Mg concentration in the carbonaceous components of the Kaidun meteorite compared to all other carbonaceous chondrites was emphasized in [32].

The genesis of individual components of clast #d6A should be considered with regard for available data on this meteorite as a whole. As is demonstrated by the results of its numerous studies [1–3], the Kaidun meteorite is characterized by the extraordinary diversity of its components. The bulk of the meteorite is made up of the material of carbonaceous chondrite of the second petrological type and contains numerous objects produced early in the evolution of the solar system: the condensation products of the nebula and the products of nebular gas metasomatism, some of which have never before been found in meteorites. At the same time, the meteorite contains clasts of alkaline and subalkaline composition, which were brought to the parent body of the meteorite during two events at different times [33]. Alkali-rich clasts are very rare in meteorites, and the occurrence of two distinct clasts of this type in the single Kaidun meteorite is hard to explain by a simple coincidence. It is more reasonable to think that the source of the alkali-rich rocks, the deep differentiation products of material in the interiors of a large planetary body, was somewhere near the parental body of Kaidun. All of these compositional features of the meteorite led us to believe that the parent body of the meteorite was a satellite of a large differentiated planet. The only possible bodies of this type in the solar system are Deimos and Phobos, satellites of Mars, of which the latter being more preferable with regard for dynamic considerations [1].

The texture and composition of inclusion #d6Aa indicate that its final evolutionary stage was marked by extensive silification of serpentine under the effect of a silicon-bearing aqueous fluid at a temperature higher than 300°C. The texture and composition of inclusion #d6Ab provide good reasons to believe that the inclusion was formed in relation to the metasomatic alteration of carbonates under the effect of Si- and Al-bearing fluids at a temperature of about 400–500°C. There are no reasons to expect that such processes, which are typical of large differentiated planets, can occur in the parent bodies of carbonaceous chondrites, such as the Kaidun meteorite. It should also be noted that the clast described in this paper contains two inclusions whose genesis was definitely related to processes in a large differentiated planet.

The characteristics of inclusions #d6Aa and #d6Ab presented above are consistent with the hypothesis that the parental body of the Kaidun meteorite was Phobos [1]. Correspondingly, inclusions #d6Aa and #d6Ab, like the alkaline clasts studied earlier, likely originated from Mars.

Inclusion #d6Ad has a mineralogy and the chemical composition of its calcite analogous to those of inclusion #d6Ab and can be of analogous genesis.

The provenance of inclusion #d6Ah, which has a crystalline habit and contains an oval polymineralic inclusion, is uncertain. On the one hand, such crystals are quite common in magmatic rocks, and, correspondingly, the precursor crystal could be borrowed from a differentiated magmatic (Martian) rock. On the other hand, analogous crystals with inclusions were also found in meteorites, including Kaidun [27].

The textures and compositions of remelted inclusions #d6Ac and #d6Ak do not provide any clues to their genesis. They could equally probably originate from small meteoritic bodies and fragments of Martian rocks ejected from the planet with high velocities at meteorite impacts.

CONCLUSIONS

The above discussion of the possible origin of inclusions in clast #d6A shows that some of them could be of Martian provenance. In this context, it is pertinent to mention that, according to calculations in [34], the concentration of Martian material in the uppermost regolith at Deimos, the second of Mars's satellites, can be as high as 10%. However, Phobos is much closer than Deimos to Mars, and the concentration of Martian material in the Phobos regolith should be much higher. Conceivably, the clast described in this publication originated from the uppermost regolith layer of Phobos that was compacted in the course of aqueous alterations of the material and later buried in a deeper layer with a lower concentration of Martian material.

ACKNOWLEDGMENTS

The authors thank S.M. Aleksandrov, B.A Bazylev, A.J. Brearley, and M.E. Zolensky for criticism and the constructive discussion of some issues considered in this paper. A. Ivanov thanks S.M. Aleksandrov for the possibility of studying his collection of rhythmically banded metasomatic rocks.

REFERENCES

1. A. V. Ivanov, "Is the Kaidun Meteorite a Sample from Phobos?" Solar Syst. Res. **38**, no. 2, 97–107 (2004)
2. A. V. Ivanov, "The Kaidun Meteorite: Composition and Evolution," Geokhimiya, No. 2, 259–266 (1989). Geochem. Int. **26**, no. 9, 84–91. (1989).
3. M. Zolensky and A. Ivanov, "The Kaidun Microbreccia Meteorite: A Harvest from the Inner and Outer Asteroid Belt," Chem. Erde **63**, 185–246 (2003).
4. *Minerals. A Handbook* (Nauka, Moscow, 1992), Vol. 4, Vyp. 1 [in Russian].
5. M. E. Zolensky, A. V. Ivanov, S. V. Yang, et al., "The Kaidun Meteorite: Mineralogy of an Unusual CM1 Lithology," Meteoritics Planet. Sci. **31**, 484–493 (1996).
6. A. J. Brearley, "Disordered Biopyriboles, Amphibole, and Talc in the Allende Meteorite: Products of Nebular or Parent Body Aqueous Alteration?," Nature **276**, 1103–1105 (1997).
7. Y. Ikeda, "Petrology and Mineralogy of the Yamato-82162 Chondrite (CI)," Proc. NIPR Symp. Antarct. Meteorites **4**, 187–225 (1991).
8. M. Kimura and Y. Ikeda, "Mineralogy and Petrology of an Unusual Belgica-7904 Carbonaceous Chondrite: Genetic Relationships Among the Components," Proc. NIPR Symp. Antarct. Meteorites **5**, 74–119 (1992).
9. A. Pabst, "The Mineralogy of Metamorphosed Serpentine at Humphreya, Fresno County, California," Am. Mineral. **27**, 570–585 (1942).
10. B. W. Evans and S. Guggenheim, "Talc, Pyrophyllite, and Related Minerals," in *Hydrous Phyllosilicates (Extrusive of Micas)*, Ed. by S. W. Bailey, Rev. Mineral. **19**, (1991)
11. W. A. Deer, R. A. Howie, and J. Zussman, *Rock-Forming Minerals. Sheet Silicates*, (Wileys, New York, 1962).
12. J. J. Hemley, J. W. Montoya, D. R. Shaw, and R. W. Luce, "Mineral Equilibria in the $MgO–SiO_2–H_2O$ System: II Talc–Antigorite–Forsterite-Anthophyllite–Enstatite Stability Relations and Some Geologic Implications in the System," Am. J. Sci. **277**, 353–383 (1977).
13. K. Bose and J. Ganguly, "Experimental and Theoretical Studies of the Stabilities of Talc, Antigorite and Phase A at High Pressures with Applications to Subduction Processes," Earth Planet. Sci. Lett. **136**, 109–121 (1995).
14. F. J. Turner, "Mineralogical and Structural Evolution of the Metamorphic Rock," Memoir. Geol. Soc. Am., 132–136 (1948).
15. I. F. Romanovich, "Formation Conditions of the Talc Deposits," in *Talc deposits of the USSR* (Nedra, Moscow, 1973), pp. 175–202 [in Russian].
16. M. Zolensky and H. Y. McSween, Jr, Aqueous Alteration," in *Meteorite and the Early Solar System*, Ed. by J. F. Kerridge and M. S. Matthews, (Univ. Arizona Press, Tuscon, 1988), pp. 114–143.
17. M. E. Zolensky, "Mineralogy and Matrix Composition of "CR" Chondrites Renazzo and EET87770, and Ungrouped Chondrites Essebi and MAC87300 (Abstract)," Meteoritics **26**, 414 (1991).
18. E. Tonui, M. Zolensky, and M. Lipschutz, "Petrography, Mineralogy and Trace Element Chemistry of Yamato-86029, Yamato-793321 and Lewis Cliff 85332: Aqueous Alteration and Heating Evens," Antarc. Meteor. Res. **15**, 38–58 (2002).
19. N. L. Bowen and O. F. Tuttle, "The System $MgO–SiO_2–H_2O$," Geol. Soc. Am. Bull. **2**, 439–460 (1949).
20. K. Metzler, A. Bischoff, and D. Stoffler, "Accretional Dust Mantle in CM Chondrites. Evidence for Solar Nebula Processes," Geochim. Cosmochim. Acta **56**, 2873–2897 (1992).
21. M. E. Zolensky, R. Barrett, and L. Browning, "Mineralogy and Composition of Matrix and Chondrule Rims in Carbonaceous Chondrites," Geochim. Cosmochim. Acta **57**, 3123–3148 (1993).
22. A. C. Moore, "Orbicular Rhythmic Layering in the Palabora Carbonatite, South Africa," Geol. Mag. **121** (1), 53–60 (1984).
23. S. M. Aleksandrov, *Geochemistry of Skarns and Ore Formation in Dolomites* (Nauka, Moscow, 1990) [in Russian].
24. S. M. Aleksandrov, "Self-Organization during Prograde Metasomatism of the Carbonate Rocks," Geokhimiya, No. 9, 1323–1338 (1995).
25. G. P. Zaraiskii, *Zoning and Formation Conditions of Metasomatic Rocks* (Nauka, Moscow, 1989) [in Russian].
26. V. V. Shcherbina, *Principles of Geochemistry* (Nedra, Moscow, 1972) [in Russian].
27. M. A. Ivanova, N. N. Kononkova, and A. V. Ivanov, "First Recorded Find of Ordinary Chondrite Material in the Kaidun Meteorite," Astronom. Vestn. **39**, 169–176 (2005) [Solar Syst. Res. **39**, 150–156 (2005)].

28. H. Nagahara, "Chondrules Formed through Incomplete Melting of the Pre-Existing Mineral Clusters and the Origin of Chondrules," in *Chondrules and Their Origins*, Ed. by E. A. King (LPI, Houston, 1983), pp. 211–222.

29. J. N. Grossman, A. E. Rubin, H. Nagahara, and E. King, "Properties of Chondrules," in *Meteorites and the Early Solar System*, Ed. by J. F. Kerridge and M. S. Mattherws (Univ. Arizona Press, Tuscon, 1988).

30. G. Kurat, E. Zinner, F. Brandstatter, and A. V. Ivanov, "Enstatite Aggregates with Niningerite, Heideite and Oldhamite from the Kaidun Carbonaceous Chondrite: Relatives of Aubrites and EH Chondrites?" Meteoritics Planet. Sci. **39**, 53–60 (2004).

31. A. T. Bazilevskii, B. A. Ivanov, K. P. Florenskii, et al., *Impact Craters on the Moon and Planets* (Nauka, Moscow, 1983) [in Russian].

32. A. V. Ivanov, A. Ya. Skripnik, A. A. Ul'yanov, et al., "Chemical Composition, Mineralogy, and Geochemical Characteristics of the New Kaidun Meteorite," Meteoritika, No. 45, 3–19 (1986) [in Russian].

33. A. V. Ivanov, N. N. Kononkova, S. V. Yang, and M. E. Zolensky, "The Kaidun Meteorite: Clasts of Alkaline-Rich Fractionated Materials," Meteoritics Planet. Sci. **38**, 725–737 (2003).

34. D. T. Britt and Gulliver Team, "The Gulliver Mission: Sample Return from the Martian Moon Deimos," Lunar Planet. Sci. **34**, 1841 (2003).